ACS APPLIED MATERIALS & INTERFACES

Research Article

www.acsami.org

Ultra-Wide-Range Electrochemical Sensing Using Continuous Electrospun Carbon Nanofibers with High Densities of States

Xianwen Mao, Xiaoqing Yang,† Gregory C. Rutledge,* and T. Alan Hatton*

Department of Chemical Engineering, Massachusetts Institute of Technology, 77 Massachusetts Avenue, Cambridge, Massachusetts 02139, United States

Supporting Information

ABSTRACT: Carbon-based sensors for wide-range electrochemical detection of redox-active chemical and biological molecules were fabricated by the electrospinning of polyacrylonitrile fibers directly onto a polyacrylonitrile-coated substrate followed by carbonization at 1200 °C. The resulting electrospun carbon nanofibers (ECNFs) were firmly attached to the substrate with good mesh integrity and had high densities of electronic states (DOS), which was achieved without need for further modifications or the use of any additives. The mass of ECNFs deposited, and thus the electroactive surface area (ESA) of the sensor, was adjusted by varying the electrospinning deposition time, thereby enabling the systematic manipulation of the dynamic range of the sensor. A standard redox probe ($Fe(CN)_6^{3-/4-}$) was used to demonstrate that the ECNF sensor exhibits strong electrocatalytic activity without current saturation at high analyte concentrations. Dopamine was used as a model analyte to evaluate the sensor performance; we find that the ECNF device exhibits a dynamic range ~10^5 greater than that of many existing carbon-based sensors. The ECNF sensors exhibited excellent sensitivity, selectivity, stability, and reproducibility for dopamine detection.

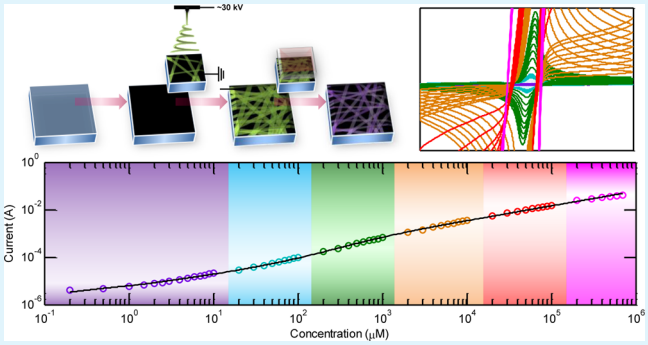

KEYWORDS: *electrochemistry, sensor, electrospinning, carbon fiber*

INTRODUCTION

Electrochemical (bio)sensors have many applications in chemical and biological industries, such as wastewater treatment, bioprocessing, clinical chemistry, and food quality control.[1] Carbon-based materials,[2−4] in particular carbon nanotubes (CNTs)[5,6] and graphene,[7,8] have attracted widespread attention for electrochemical sensing because of their adjustable electrocatalytic activities toward various redox-active species. Considerable effort has been expended to improve the limit of detection (LOD).[1−8] The dynamic range, another important aspect of sensor performance, is the analyte concentration range over which the sensor can operate within acceptable limits of distortion and is ultimately determined by the system noise at the lower end (i.e., LOD) and by the onset of signal saturation at the upper end. Broad sensing ranges are particularly important for detection of undiluted, real-world samples with a wide range of concentrations, with applications in pharmaceutical analysis,[9] food regulation,[10] water monitoring,[1] and in vivo measurements in biological media.[11−13] To the best of our knowledge, only one study has focused on the expansion of the dynamic range of sensors, which used dual-fluorescence-quenching mechanisms.[14] However, this method cannot be applied generally to redox-active systems with significance in various chemical industries, such as pharmaceutical compounds, toxic metals, pesticides residuals, dye molecules, and biologically relevant systems (e.g., neurochemicals, proteins, and DNA).[1,5,8−10] To date, there is no study dealing with expanding the dynamic ranges of electrochemical sensing devices.

For electrochemical sensors, the electroactive surface area (ESA) is the key determinant of the upper bound of the dynamic range. A larger ESA can postpone current saturation to a higher analyte concentration, leading to an increased upper limit. Most carbon-based electrochemical sensors possess inherently narrow dynamic ranges, mainly because of their limited ESAs. Conventional electrodes such as glassy carbon (GC), carbon paste electrodes (CPE), and microfabricated carbon films have nonporous structures and low ESAs.[2] It is possible to increase ESAs to a certain degree by depositing CNTs or graphene onto flat substrates to create porous structures. However, as-synthesized CNTs and graphene are generally small and discontinuous; therefore, proper assembly methods for the integration process are necessary. Common assembly strategies include solution casting,[15,16] layer-by-layer assembly,[17] sol−gel transition,[18] covalent modification,[19] and electrochemical co-deposition.[20] However, these methods generally lead to low loadings of electroactive materials (a few micrograms per electrode for electrode surface areas of ~1

Received: November 29, 2013
Accepted: February 19, 2014
Published: February 19, 2014

 © 2014 American Chemical Society

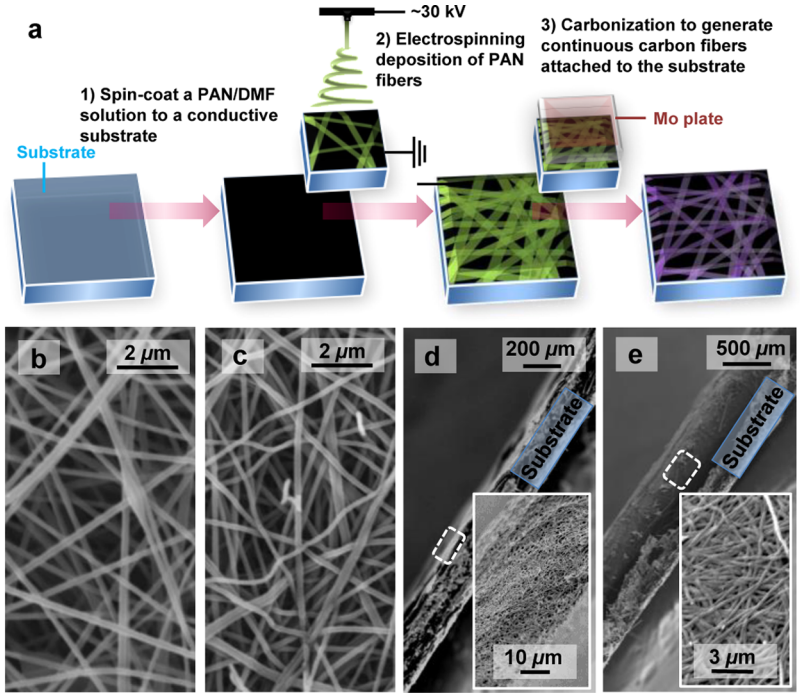

Figure 1. (a) Schematic illustration of the sensor-fabrication process. (b, c) SEM images of (b) as-spun PAN fibers and (c) carbonized fibers. (d, e) Cross-sectional SEM images of the ECNF sensors with a deposition time of (d) 12 and (e) 68 h. Insets are the enlarged dotted rectangles.

cm^2), resulting in limited ESAs of the sensors ($\sim 10^{-2}$ cm^2). Moreover, pristine CNTs and graphene need modification to create linkable groups and/or to generate edge sites for high electrochemical sensitivity. These modifications make such processes inefficient, expensive, and difficult to scale up. Additionally, most fabrication procedures involve the use of electrochemically inert components such as surfactants and binders, which may hinder transport of electrons, ions, and analytes, leading to reduced sensor performance.

Large electroactive surface areas have been generated effectively through the treatment of carbon fibers with high anodic currents or potentials.[21,22] Alternatively, our work focuses on use of electrospinning and subsequent thermal treatment to fabricate carbon electrodes with high ESAs. Electrospinning is a simple, efficient, and scalable technique for the generation of continuous fibers.[23] Thermal treatment can convert electrospun fibers of certain polymers (e.g., polyacrylonitrile (PAN)) to carbonaceous nanofibers.[24] To date, electrochemical applications of electrospun carbon nanofibers (ECNFs) have been dominated by energy storage,[24,25] and only a few studies have examined their electrochemical sensing properties.[26,27] These sensors were fabricated by conventional solution-cast methods using suspensions containing broken, discontinuous ECNFs, with electrocatalytic activities governed by additives such as palladium[26] and rhodium[27] nanoparticles incorporated within the fiber matrices.

In this work, continuous all-carbon ECNFs have been developed for electrochemical sensing applications with wide dynamic ranges and high sensitivities. The ECNF sensors were fabricated by the electrospinning of PAN fibers directly onto conductive substrates followed by carbonization at 1200 °C.[28] This process allows firm attachment of a controllable amount of continuous ECNFs to the substrate without the use of binders. As a result, the ESAs of the sensors can be adjusted easily by control of the electrospinning deposition time, which enables systematic manipulation of the dynamic range of the sensor. Another unique aspect of the ECNF sensors is that their high sensitivities are readily achieved through thermal treatment at 1200 °C without the need for further modifications of the carbonized fibers or the use of other noncarbon components. Previously, we have shown that ECNFs carbonized from PAN at 1200 °C exhibit abundant edge defects and high densities of electronic states (DOS).[28] Such unique features of ECNFs distinguish them from the commercial carbon fibers most commonly used industrially in structural materials, which rely on a high degree of graphitization to remove edge defects and to maximize the tensile strength.[2] We find that the ECNFs developed here exhibit significantly better electrocatalytic performance than that observed with commercially available graphitized fibers (GFs). Moreover, our sensor-fabrication method creates a conductive carbon network with high porosity. This structure is desirable for electrochemical sensing because it can simultaneously facilitate electron transport in the conductive framework and promote analyte diffusion in the pores.[29−31] Furthermore, the ECNF sensing platform can apply to a plethora of analytes because the electron-transfer efficiencies of many redox species and biomolecules are largely dictated by the DOS of the electrode materials.[2,28,32]

As proof of principle, we used dopamine (DA) as a model analyte to evaluate the sensor performance. DA is an important neurotransmitter with a crucial role in human metabolism as well as in the cardiovascular, central nervous, renal, and hormonal systems[33,34] and can shed light on the treatment of schizophrenia, Huntington's disease, and Parkinson's disease.[35−37] Advanced carbon electrodes,[2] especially those based on CNTs[20,38−48] and graphene,[15,16,49−53] have been researched extensively for electrochemical DA detection, and the detection ranges of these DA sensors have been well-documented. The ECNF sensors developed here demonstrate remarkably wide sensing ranges (up to the solubility limit of DA) while exhibiting detection limits comparable to those of sensors currently reported in the literature. Although there is

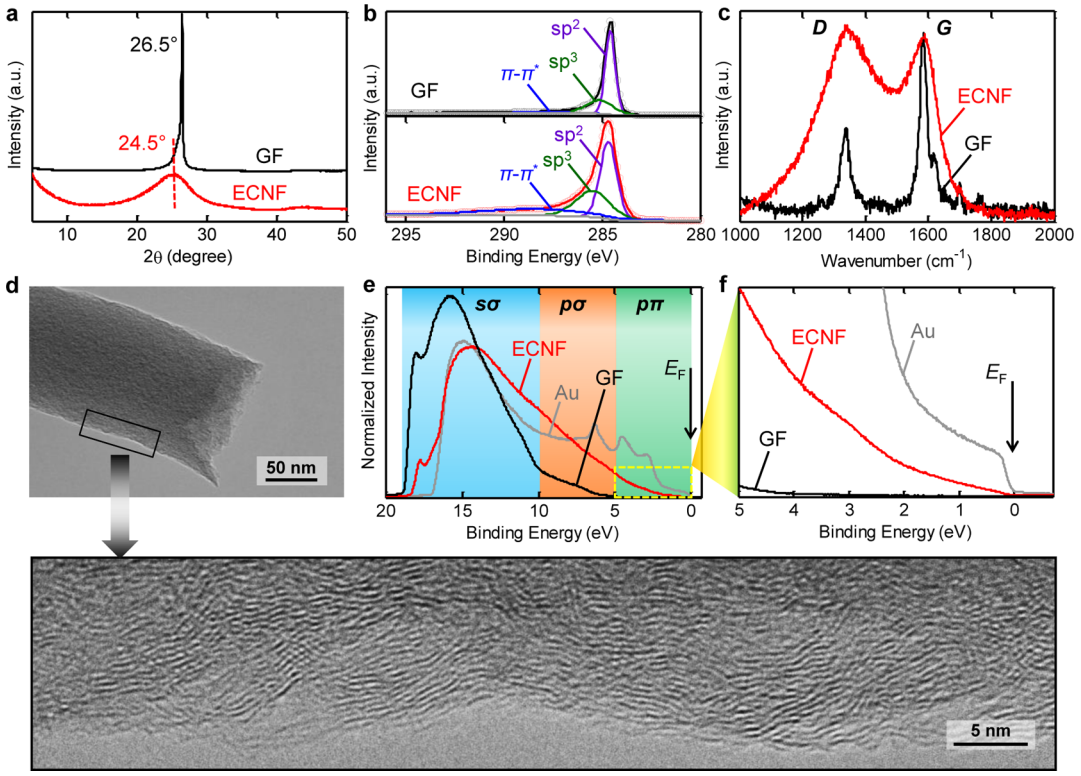

Figure 2. (a) XRD patterns showing the shifting and broadening of the (002) peak of ECNFs relative to GFs. (b) High-resolution C 1s XPS spectra showing a higher sp^3/sp^2 ratio for ECNFs than for GFs. (c) Raman spectra showing a higher R_I value for ECNFs than for GFs. (d) HR-TEM image of an individual ECNF showing irregularly oriented graphene sheets. (e) UPS spectra of ECNFs and GFs showing their electronic structures. Gold was used as the internal standard to locate the Fermi level. (f) Details of the UPS spectra near the Fermi level showing a much higher DOS at E_F for ECNFs than for GFs.

little or no practical need for detection of DA at high concentrations, the results bode well for the development of electrochemical sensors with broad detection ranges that are potentially useful for monitoring several other substances that are present with high concentrations, such as soluble dyes in highly polluted textile industrial wastewater,[1] nonbiodegradable pesticides that persist and accumulate in the environment,[10] and pharmaceutically active compounds in bulk drug materials and drug formulations.[9]

RESULTS AND DISCUSSION

Fabrication and Microstructural Characterization of the ECNF Sensor. Figure 1 shows the sensor fabrication process schematically (also see the Experimental Section). Briefly, a conductive substrate is coated with a thin PAN film by spin-coating followed by the electrospinning deposition of PAN nanofibers. Toray carbon papers composed of GFs are used as the substrate because they are stable during high-temperature treatment. The PAN film serves as the glue to prevent fiber detachment from the substrate after carbonization. Next, the PAN components of the substrate/film/nanofiber construct are carbonized at a temperature of 1200 °C. This temperature has previously been shown to be optimal for imparting the resulting ECNFs with high DOS.[28]

A representative scanning electron microscopy (SEM) image of the as-spun PAN fibers (Figure 1b) shows that their diameters are around 300 nm. The carbonized fibers have slightly smaller diameters of ~250 nm (Figure 1c) because of the mass loss associated with evolved gases.[54] The cross-sectional SEM images of the ECNF sensors with different deposition times are shown in Figure 1d,e. The ECNFs are densely packed and firmly attached to the substrate. This suggests that our fabrication procedure is effective in producing substrate-supported porous meshes composed of interconnected carbonaceous nanofibers without using binders. The loading of the electroactive materials (i.e., ECNFs) can be easily adjusted through the deposition time. With an increase from 12 to 68 h, the thickness of the ECNF mesh increases from ~60 to ~500 μm without loss of mesh integrity. The ability to control the loading mass of ECNFs is significant for ESA manipulation to achieve optimum sensing performance. The ESAs of the ECNF devices as a function of deposition time can be determined by electrochemical methods, as will be discussed later.

The ECNFs developed here exhibit a microstructure that is drastically different from that of GFs. X-ray diffraction (XRD) measurements (Figure 2a) show that the peak representing the (002) graphitic basal-plane reflection for the ECNFs is observed at a lower 2θ value (24.5°) relative to that for GFs (26.5°). Additionally, the diffraction peak for ECNFs is much broader than that for GFs. The average interlayer spacing (d_{002}) and the crystallite size (L_c) were estimated using the Bragg and Scherrer equations, respectively.[54] The d_{002} for GFs was found to be 0.336 nm, in accordance with the value for isotropic graphite.[55] ECNFs have a larger d_{002} value of 0.354 nm, indicating that ECNFs display turbostratic carbon structures with a low graphitization degree. The L_c value for GFs (22.5 nm) is larger than that for ECNFs (1 nm), indicating that ECNFs contain smaller crystallites.

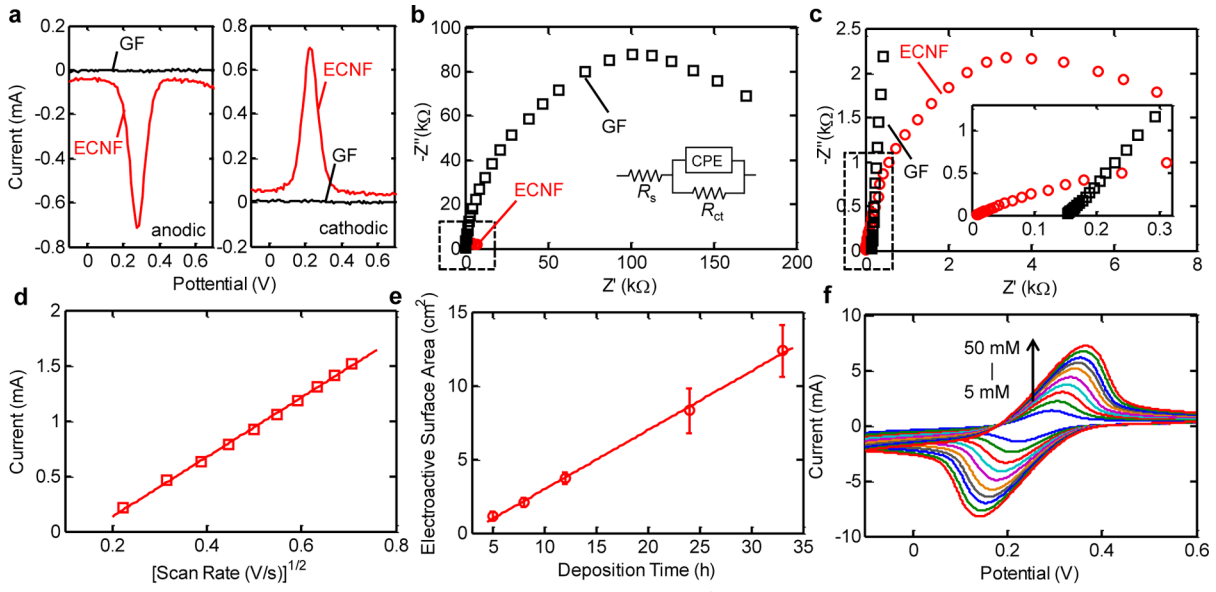

Figure 3. Electrochemical evaluation using $Fe(CN)_6^{3-/4-}$. (a) Anodic and cathodic DPVs. (b) Nyquist plots showing the difference in R_{ct} and R_s between the ECNF sensor and the GF substrate. Inset shows the equivalent circuit used to model the impedance data. R_s, electrolyte solution resistance; R_{ct}, interfacial charge-transfer resistance; and CPE, constant phase element. (c) Enlarged view of the dotted rectangle in panel b. Inset shows the enlarged dotted area in panel c, revealing the intercepts on the Z' axis. (d) Peak current from CVs versus the square root of scan rate showing the semi-infinite linear diffusion behavior of $Fe(CN)_6^{3-/4-}$ on the ECNF sensor. (e) Calculated ESAs as a function of electrospinning deposition time. For the measurements in panels a–e, the solution contains 1 mM $Fe(CN)_6^{3-/4-}$ in 1 M KCl. (f) CVs obtained on the ECNF sensor (12 h deposition) at high concentrations of $Fe(CN)_6^{3-/4-}$ ranging from 5 to 50 mM.

High-resolution C 1s X-ray photoelectron spectra (XPS) (Figure 2b), deconvoluted into sp^2, sp^3, and $\pi-\pi^*$ components,[56] indicate that ECNFs have a higher sp^3/sp^2 ratio (0.7) than GFs (0.4). Raman spectra (Figure 2c) show that the R_I value (the intensity of the D band at 1337 cm^{-1} divided by that of the G band at 1585 cm^{-1})[57] is higher for ECNFs (1.26) than for GFs (0.47). The XPS and Raman results confirm that ECNFs contain more edge-like defects than GFs. For calculation of the sp^3/sp^2 and R_I values, see the Supporting Information. Figure 2d shows a representative high-resolution transmission electron microscopy (HR-TEM) image of the edge of an ECNF. The fiber surface exhibits a wrinkled topology with irregular orientation of stacked graphene sheets. In contrast, the surfaces of completely graphitized fibers contain mostly graphite basal planes and very few edge-plane sites.[2]

We hypothesize that ECNFs provide a higher DOS than GFs because the defect-rich nature of ECNFs may result in greater overlap between the valence and conduction bands.[58] To test this hypothesis, He(I) ultraviolet photoemission spectroscopy (UPS) was used to probe directly the electronic structure of ECNFs and GFs; the normalized UPS intensity corresponds to the DOS of the materials investigated.[59] The UPS spectra normalized with respect to the total integrated intensities (Figure 2e) show that both GFs and ECNFs exhibit graphite-like valence-band structures. The intensities from 0–5, 5–10, and 10–18 eV are attributed to $p\pi$-, $p\sigma$-, and s-like σ bands, respectively.[60] More importantly, Figure 2f indicates that ECNFs have a higher DOS near the Fermi level (0 eV) than GFs. The DOS of electrode materials near the Fermi level plays a crucial role in their electrochemical activities.[2,61]

Electrochemical Evaluation Using an Edge-Site-Sensitive Redox Probe and Determination of Electroactive Surface Area. Ferrocyanide–ferricyanide ($Fe(CN)_6^{3-/4-}$) has been adopted frequently as the standard redox couple to study the electrochemical activities of various electrode materials.[2] For carbon materials, this redox probe is of particular interest because its electron-transfer process depends strongly on the density of edge sites on carbon surfaces.[2,62] Figure 3a shows the anodic and cathodic differential pulse voltammograms (DPVs) of a bare GF substrate and an ECNF sensor in 1 mM $Fe(CN)_6^{3-/4-}$. The GF substrate exhibits almost no current response. By contrast, the ECNF sensor displays a pronounced anodic peak of −0.71 mA at 0.27 V and a sharp cathodic peak of 0.70 mA at 0.23 V. Carbon microstructures influence significantly the electrochemical activities of carbon electrodes.[2] The basal planes of graphite electrodes have been shown to display very low activity[63,64] or even no electroactivity.[65−68] Therefore, one of the possible reasons for the higher electrochemical activity of ECNFs relative to that of GFs may be the higher edge-site density of ECNFs. In addition, $Fe(CN)_6^{3-/4-}$ is very sensitive to the state of the carbon surface; a nitrophenyl monolayer on GC caused a significant decrease in its activity toward $Fe(CN)_6^{3-/4-}$.[69] The observed electrochemical inertness of GFs in our experiments was determined not to be because of inadvertent adsorption of impurities, however, since no current response toward $Fe(CN)_6^{3-/4-}$ was observed with either new GF substrates or with GF substrates cleaned carefully by a standard cleaning procedure using activated carbon and sonication (see Experimental Section).[70]

Electrochemical impedance spectroscopy (EIS) was adopted to measure the interfacial charge-transfer resistance (R_{ct}) and the solution resistance (R_s). In EIS spectra, the diameter of the semicircle and the intercept on the Z' axis approximate the R_{ct} and R_s values, respectively. The spectrum of the ECNF sensor (Figure 3c, red symbols) is characterized by a semicircle with impedance values that are significantly lower than those obtained on the bare GF substrate (Figure 3b, black symbols) (i.e., R_{ct} for the ECNF sensor is reduced compared to that of the GF substrate). The inset in Figure 3c shows that R_s for the

dx.doi.org/10.1021/am405461j | ACS Appl. Mater. Interfaces 2014, 6, 3394−3405

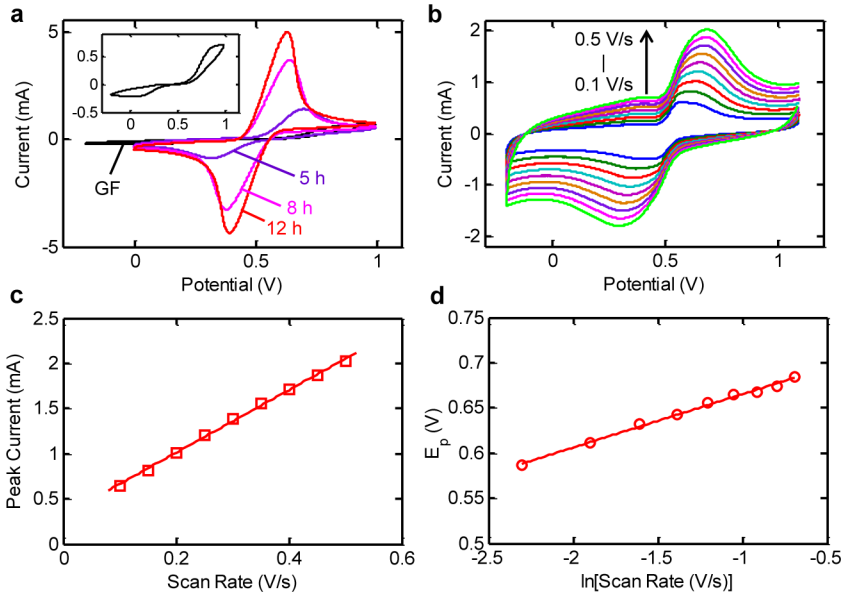

Figure 4. (a) CVs of the GF substrate and the ECNF sensors with different deposition times obtained at a scan rate of 0.05 V/s in 10 mM DA. Inset shows the enlargement of the CV curve obtained on the GF substrate. (b) CVs obtained on an ECNF sensor (12 h) in 1 mM DA at scan rates from 0.1 to 0.5 V/s. (c) Anodic peak current versus scan rate. (d) Anodic peak potential versus the natural logarithm of scan rate. Results shown in panels c and d indicate that the redox reaction of DA on the ECNF sensor is surface-controlled.

ECNF sensor is ~0 kΩ, much lower than that for the GF substrate (~ 0.15 kΩ). An equivalent circuit (Figure 3b, inset) is used to fit the impedance data to calculate the R_{ct} and R_s values. Significantly lower values for both parameters are obtained on the ECNF device (R_{ct} = 6.5 ± 0.2 kΩ and R_s = 0 kΩ) compared to those obtained on the GF substrate (R_{ct} = 193.6 ± 3.1 kΩ and R_s = 0.15 kΩ). The DPV and EIS evaluations are consistent with the presence of an abundance of edge-plane sites on ECNFs, whereas GFs contain relatively fewer such electroactive defects. These electrochemical measurements are in agreement with the microstructural comparison between the two types of material systems.

Well-defined cyclic voltammetric (CV) responses for an ECNF sensor in 1 mM $Fe(CN)_6^{3-/4-}$ at varying scan rates (Figure S2) suggest that this device can support quasi-reversible electron-transfer kinetics for this redox probe. A linear relationship between the anodic peak current and the square root of scan rate (Figure 3d) indicates a diffusion-controlled, not surface-limiting, charge-transfer behavior with $Fe(CN)_6^{3-/4-}$. This current response was controlled by the planar diffusion of redox molecules present between the fibers or inside the pores of the fibrous mat to the fiber surfaces themselves (see Supporting Information section S6 for a detailed discussion) and thus the results of the $Fe(CN)_6^{3-/4-}$ scans can be used to estimate the ESA of the sensing device based on the Randles–Sevcik equation[71]

$$I_p = 2.69 \times 10^5 A D^{1/2} n^{3/2} C v^{1/2} \quad (1)$$

where I_p is the peak current (mA), A is the ESA of the electrode investigated (cm^2), D is the diffusion coefficient of ferricyanide (7×10^{-6} cm^2/s),[71] n is the number of electrons transferred in the redox reaction of $Fe(CN)_6^{3-/4-}$, C is the concentration of ferricyanide in the bulk solution (M), and v is the scan rate (V/s). The ESA value is calculated from the slope of the I_p versus $v^{1/2}$ linear regression equation.

Figure 3e shows the ESAs of the ECNF sensors with different electrospinning deposition times. The ECNF device with a deposition time of 12 h exhibits an ESA of 3.7 cm^2, a value that is significantly higher than that reported for electrochemical biosensors based on CNT assemblies (generally ~10^{-2} cm^2).[72] Additionally, there exists a linear correlation between the ESA values and the deposition time, which indicates that the ESA can be controlled systematically using our fabrication process.

To show that a high ESA postpones current saturation and thus expands the sensing range of the detector, we increased the concentration of $Fe(CN)_6^{3-/4-}$ to higher values and measured the corresponding current responses of the ECNF sensor prepared with a 12 h deposition time. Figure 3f shows the CV responses obtained on the sensor at different $Fe(CN)_6^{3-/4-}$ concentrations, ranging from 5 to 50 mM. Whereas the peak current increases monotonically with the analyte concentration, the current signal increment with fixed increments in concentration gradually decreases, which indicates that current saturation might occur if the concentration of $Fe(CN)_6^{3-/4-}$ is sufficiently high. Nevertheless, the upper bound of the detection range achieved on the ECNF sensor appears to be much higher than those reported to date with other electrochemical sensors.

Electrocatalysis against Dopamine. The well-documented performance of sensors for the widely studied model analyte dopamine (DA) provides a strong basis for evaluation of the ECNF sensors developed in this work. Figure 4 shows the CV curves in 10 mM DA solutions obtained on a bare GF substrate and several ECNF sensors with different deposition times. The unmodified GF substrate shows ill-shaped voltammetric responses with a pair of weak peaks around 0.9 and 0.1 V (Figure 4a inset). By contrast, the CV curves obtained on the ECNF sensors are characterized by sharp, well-defined redox peaks. These results indicate that the ECNF sensors display much higher electrochemical activity toward DA. Additionally, we observe that the magnitude of the current signals increases with deposition time. From 5 to 8 to 12 h, the anodic peak currents increase from 1.6 to 3.7 to 5.0 mA, and

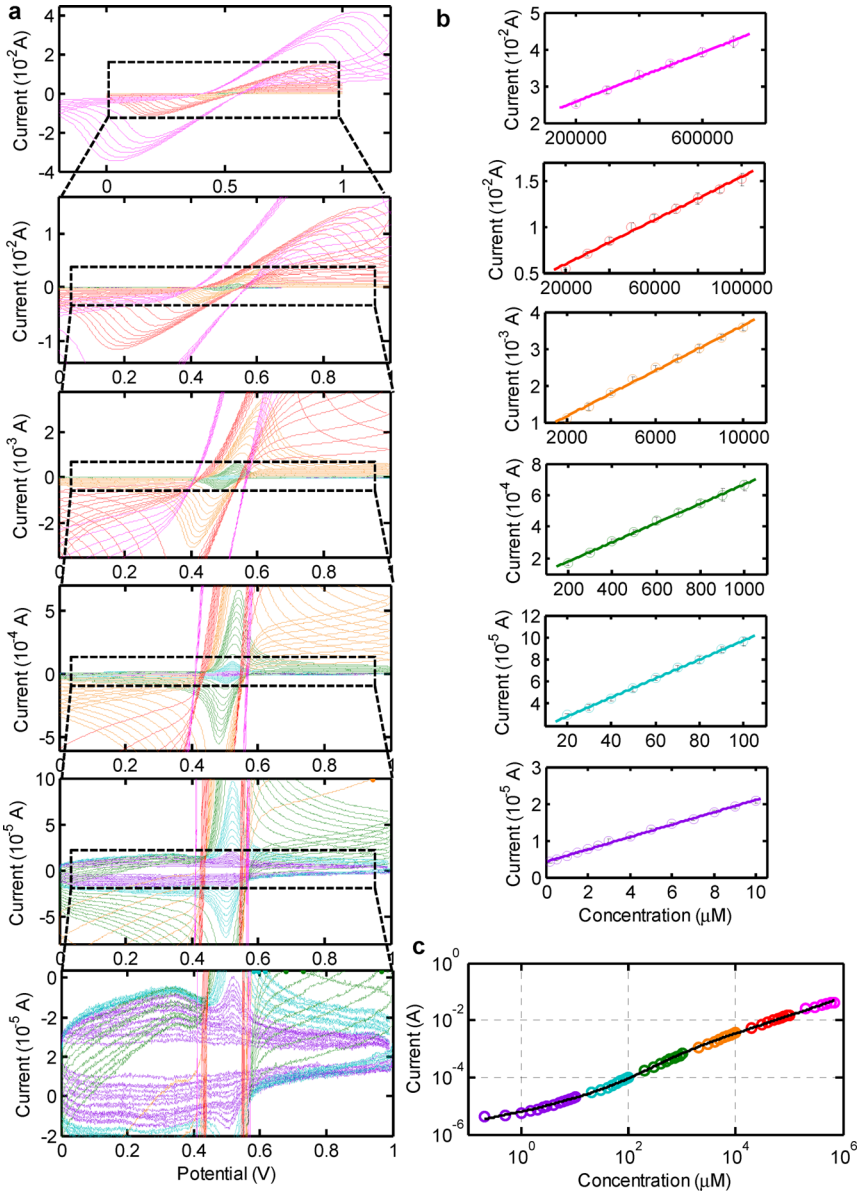

Figure 5. (a) Background-subtracted CV responses of an ECNF sensor (12 h deposition) obtained over different concentration ranges. From top to bottom: 200 000−700 000, 20 000−100 000, 2 000−10 000, 200−1000, 20−100, and 0.2−10 μM. (b) Piecewise linear fitting for different concentration ranges. (c) Continuous nonlinear fitting for the whole concentration range.

the cathodic peak currents increase from 0.9 to 3.2 to 4.4 mA, respectively. This higher current density is consistent with an increased ESA. Furthermore, the value of the peak-to-peak separation (ΔE_p) in the CVs decreases from 400 to 270 to 220 mV with increasing deposition time. The ECNF sensor with a higher ESA displays a more reversible electron-transfer process for DA, indicated by a lower ΔE_p value. DA requires adsorption to realize efficient electron transfer and thus its electrochemical kinetic behavior can be improved significantly by increasing the electrode ESAs.[73,74]

Mechanistically, the interplay between dopamine and an electrode can be probed by examining the voltammetric response of the electrode at varying scan rates, ν. Figure 4b shows the influence of ν on the CV response of an ECNF sensor to 1 mM DA. With increasing ν, both the anodic and cathodic peak currents increase gradually, whereas the anodic and cathodic peak potentials shift to more positive and negative positions, respectively. Figure 4c shows that the anodic peak current (I_{pa}) increases linearly with ν. The resulting regression equation is

$$I_{pa}\ (\mathrm{mA}) = 3.5\nu\ (\mathrm{V/s}) + 0.3 \quad (r^2 = 0.999) \tag{2}$$

This linearity between I_{pa} and ν signifies that the electrochemical reaction of DA on the ECNF sensor is controlled by surface adsorption. We also observe a linear relationship between the anodic peak potentials (E_{pa}) and ln ν (Figure 4d), with a regression equation expressed as

$$E_{pa}\ (\mathrm{V}) = 0.059 \ln \nu\ (\mathrm{V/s}) + 0.724 \quad (r^2 = 0.982) \tag{3}$$

consistent with the Laviron model,[75] which predicts that, for a surface-controlled redox reaction, E_{pa} and ln ν are linearly correlated.

Wide-Range Dopamine Detection. To demonstrate ultra-wide-range detection of DA, we varied its concentration from 0.2 to 700 000 μM and recorded the corresponding

dx.doi.org/10.1021/am405461j | ACS Appl. Mater. Interfaces 2014, 6, 3394−3405

voltammetric response of the sensors. The highest concentration approaches the solubility of DA in water (~ 1 M) at room temperature. If the ECNF sensor provides a sufficiently high ESA, then the current should not saturate at the highest DA concentrations used. Therefore, a strictly increasing calibration function between the current signal and the analyte concentration should be obtained. Figure 5a shows the background-subtracted CV response of an ECNF sensor (12 h deposition). From top to bottom, the overlaid CV curves are enlarged stepwise to show clearly the voltammetric responses obtained over different concentration ranges, indicated by different colors. The CV curves are well-resolved at low DA concentrations (0.2−10 μM, purple lines) and do not become saturated even at DA concentrations approaching the solubility limit (200 000−700 000 μM, pink lines); thus, the sensor exhibits a low LOD and a wide dynamic range. Figure 5b shows piecewise linear fitting between I_{pa} and the DA concentration (C_{DA}). The $I_{pa} - C_{DA}$ relationship is linear over a concentration range of approximately 1 order of magnitude. Table 1

Table 1. Linear Calibration Curves for DA Detection over Different Concentration Ranges Using an ECNF Sensor[a]

concentration regime [μM]	linear regression equation I_{pa}, [A]; C_{DA}, [μM]	r^2
200 000−700 000	$I_{pa} = 3.33 \times 10^{-8} C_{DA} + 1.91 \times 10^{-2}$	0.9978
20 000−100 000	$I_{pa} = 1.19 \times 10^{-7} C_{DA} + 3.53 \times 10^{-3}$	0.9962
2000−10 000	$I_{pa} = 3.09 \times 10^{-7} C_{DA} + 5.47 \times 10^{-4}$	0.9982
200−1000	$I_{pa} = 6.13 \times 10^{-7} C_{DA} + 5.58 \times 10^{-5}$	0.9988
20−100	$I_{pa} = 8.57 \times 10^{-7} C_{DA} + 1.13 \times 10^{-5}$	0.9994
0.2−10	$I_{pa} = 1.69 \times 10^{-6} C_{DA} + 4.20 \times 10^{-6}$	0.9986

[a]Twelve hour deposition.

summarizes the corresponding linear regression equations and correlation coefficients for different C_{DA} ranges. The LOD value of the ECNF sensor was determined to be 0.08 μM (at a signal-noise ratio of 3) on the basis of the following equation

$$\mathrm{LOD} = \frac{3\sigma}{S} \tag{4}$$

where σ is the standard deviation of five measurements of the blank solution and S is the slope of the linear regression equation for the lowest concentration range (i.e., 0.2−10 μM). Linear fitting over the entire concentration range would not be accurate because the slope of a piecewise linear fit for each concentration range changes from 1.69×10^{-6} for the lowest concentration range to 3.33×10^{-8} for the highest concentration range. To obtain a continuous calibration curve for the entire C_{DA} range, we plot the $I_{pa} - C_{DA}$ data on a log−log plot (Figure 5c) where the data exhibit a quasi-linear form with an S shape. Using a linear function (i.e., $\beta_1 + \beta_2 x$) to fit the $\ln C_{DA} - \ln I_{pa}$ data, a root-mean-square deviation (rmsd) of 0.22 was obtained. By adding a sigmoid function term, $((\beta_3)/(1 + \exp(-x + \beta_4)))$, we obtained an improved rmsd of 0.14. After further incorporating a higher-order term, $\beta_5 x^{\beta 6}$ ($\beta_6 > 1$), a low rmsd of 0.06 was achieved. The resulting nonlinear regression equation including all three terms, plotted as a solid line in Figure 5c, describes well the experimental data over the entire concentration range. The nonlinear fitting results are summarized in Table 2.

Next, we compare the dynamic ranges and LOD values of the ECNF sensors manufactured with different deposition times (Table 3). The sensing performance improves markedly (i.e., a

Table 2. Nonlinear Fitting Results for DA Detection over the Entire Concentration Range from 0.2 to 700 000 μM

nonlinear fitting function form I_{pa}, [A]; C_{DA}, [μM]	values of the fitting coefficients	root-mean-square deviation (rmsd)
$\ln I = \beta_1 + \beta_2 \ln C_{DA}$	$\beta_1 = -12.25$, $\beta_2 = 0.70$	0.22
$\ln I_{pa} = \beta_1 + \beta_2 \ln C_{DA} + \beta_3/(1 + \exp(-\ln C_{DA} + \beta_4))$	$\beta_1 = -9.08$, $\beta_2 = 0.72$, $\beta_3 = -3.39$, $\beta_4 = -2.14$	0.14
$\ln I_{pa} = \beta_1 + \beta_2 \ln C_{DA} + \beta_3/(1 + \exp(-\ln C_{DA} + \beta_4)) + \beta_5(\ln C_{DA}) + \beta 6$	$\beta_1 = -11.99$, $\beta_2 = 0.25$, $\beta_3 = 1.36$, $\beta_4 = 5.60$, $\beta_5 = 0.19$, $\beta_6 = 1.20$	0.06

Table 3. Limits of Detection (LOD) and Dynamic Ranges of the ECNF Sensors with Different Electrospinning Deposition Times

deposition time [h]	limit of detection [μM]	dynamic range [μM]
5	5.58	8−9000
8	1.52	3−50 000
12	0.08	0.2−700 000
24	0.08	0.2−700 000
33	0.07	0.2−700 000

lower LOD and a wider dynamic range) when the deposition time increases from 5 to 12 h. The expanded detection range is a direct result of a higher ESA of the device that postpones current saturation. The lower detection limit with increasing deposition time (and thus increasing ESA) is a consequence of the electron-transfer mechanism with dopamine. Dopamine is an inner-sphere species whose redox reaction is surface-sensitive and adsorption-assisted; thus, a large electrode surface area increases electron-transfer efficiencies with DA and results in enhanced sensitivity.[2] It should be pointed out that in the cases in which the deposition time is 12, 24, or 33 h the current response does not necessarily become saturated above 700 000 μM; rather, this upper bound is due to the solubility limit of DA in water. Further increases in deposition time beyond 12 h do not lead to a significantly improved detection limit. The ECNF sensors with 24 and 33 h deposition time have LODs of 0.08 and 0.07 μM (S/N = 3), respectively. These values are similar to the detection limit obtained with an ECNF sensor prepared with a 12 h deposition time. When the deposition time exceeded 12 h, both the slope of the calibration curve and the system noise increased simultaneously. That is, according to eq 4, with an increase in both S and σ, the LOD value does not necessarily decrease. Moreover, as shown in Figure 3e, the standard deviations of the sensor ESAs with 24 and 33 h deposition times are larger than that with 12 h deposition. Thus, the ECNF sensor with 12 h deposition demonstrates better reproducibility compared to those fabricated with longer deposition times.

Figure 6 compares an ECNF sensor (12 h deposition) with previously reported electrochemical biosensors based on carbon nanotubes[20,38−48] (green data) and graphene[15,16,49−53] (blue data) for dopamine detection. Most of these biosensors were manufactured by casting CNT- or graphene-containing suspensions onto conventional nonporous electrodes such as GC.[15,16,39,42,44−46,48,50−53] Other fabrication methods have also been used, including layer-by-layer assembly,[43,47] covalent binding,[38] mixing with carbon paste,[41,49] direct growth of CNTs,[40] and electrochemical deposition.[20] It is apparent that the ESAs of the resulting sensors are fairly limited regardless of the assembly strategy. This leads to relatively narrow sensing

dx.doi.org/10.1021/am405461j | ACS Appl. Mater. Interfaces 2014, 6, 3394−3405

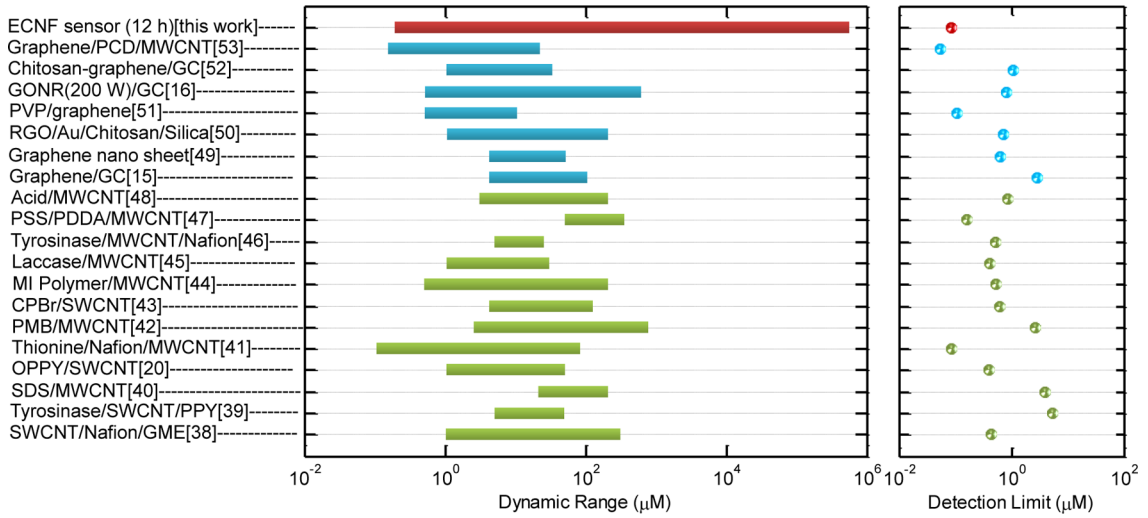

Figure 6. Comparison of the dynamic range and the detection limit between the ECNF sensor (12 h) and previously reported electrochemical biosensors based on graphene (blue) and carbon nanotubes (green). Abbreviations (from bottom to top): SWCNT, single-walled carbon nanotube; GME, conical glass micropore electrode; PPY, polypyrrole; SDS, sodium dodecyl sulfate; MWCNT, multiwalled carbon nanotube; OPPY, overoxidized polypyrrole; PMB, poly(methylene blue); CPBr, cetylpyridinium bromide; MI, molecularly imprinted; PSS, polystyrene sulfonate; PDDA, poly(diallyldimethylammonium chloride); RGO, reduced graphene oxide; PVP, poly(vinylpyrrolidone); GONR, graphene oxide nanoribbon; GC, glassy carbon; and PCD, polycyclodextrin.

ranges that are generally smaller than 2 orders of magnitude (Figure 6). By contrast, the ECNF sensor exhibits a remarkably wider sensing range, spanning more than 6 orders of magnitude. As noted earlier, although the detection of DA at these high concentrations is not generally necessary, these results indicate that other electrochemical sensors with similar broad detection ranges may be prepared for monitoring several other substances that are present with high concentrations, such as soluble dyes in highly polluted textile industrial wastewater,[1] nonbiodegradable pesticides that persist and accumulate in the environment,[10] and pharmaceutically active compounds in bulk drug materials and drug formulations.[9]

In addition, to achieve high sensitivity, the CNT- and graphene-based biosensors usually require further modifications of the carbon materials and/or introduction of other noncarbon active components. These modifications are necessary because pristine carbon nanotubes and graphene contain very few electroactive edge defects and thus exhibit limited catalytic activities.[5−8] For dopamine sensing, most previous studies focus on incorporation of noncarbon components, including enzymes,[39,45,46] functional polymers,[20,40,42,44,51−53] and metal nanoparticles.[50] To the best of our knowledge, only one report[16] concentrates on manipulation of carbon structures and generation of edge sites; in this case, microwave energy was used to exfoliate multiwalled carbon nanotubes. Our as-synthesized ECNFs possess more surface edge sites with fewer processing steps than CNTs and graphene[28] and offer a significantly lower LOD value (0.08 μM) than pristine graphene-based sensors (2.64 μM).[15] The sensitivity of the ECNF sensor is better than, or comparable to, the sensitivities of the sensors based on modified CNTs and graphene (Figure 6). Moreover, in control experiments, we found that the GF electrode has a much narrower dynamic range than the ECNF sensor (see Supporting Information section S7). The low activity of the GF electrode is attributed to a lack of edge sites, low DOS, and small microscopic surface area (which is reflected by the much lower capacitance of the GF electrode compared to that of the ECNF sensor, see Supporting Information section S8).

The ECNF sensors show satisfactory reproducibility, stability, and selectivity. Five successive CV measurements using the same sensor for detection of 0.1 mM DA yield a relative standard deviation (RSD) of 1.3%, indicating excellent repeatability. The RSD for five ECNF sensors manufactured under the same conditions (12 h deposition time) is 5.9%, suggesting reasonable fabrication reproducibility. After being stored in an open laboratory atmosphere for 1 month, 95.6% of the initial CV response (i.e., the magnitude of the anodic peak current) to 0.1 mM DA remains, suggesting good sensor stability. After each measurement, the sensor was rinsed thoroughly with deionized water and ethanol. The good stability and ease of storage is attributed to the nonenzymatic nature of the ECNF sensor.[39,45,46] It has been reported that the CV response for DA detection decays greatly (more than 95%) immediately after the first scan cycle, possibly because of fouling of the electrode surface by the oxidized DA products (such as dopaminechrome and melanin).[76] This is not the case for our ECNF device. After 20 CV cycles, the magnitude of the anodic peak current remains almost unchanged with 1 and 10 mM DA present (Figure S2a,b) and decays marginally (5%) even at a very high dopamine concentration of 100 mM (Figure S2c). We attribute this to the high ESA of the sensor, which can sustain stable voltammetric signals despite possible surface contamination with repeated cycling. For the selectivity of electrochemical DA sensors, a major challenge is to eliminate the interference from ascorbic acid (AA),[15,38,41,44,77,78] which coexists with DA in brain tissues and biological fluids and exhibits an oxidation peak potential very close to that of DA at conventional electrodes such as Au, Pt, and glassy carbon electrodes.[79] On the ECNF sensor, we find that the current response from AA is significantly lower than that from DA at the same concentration and that there is complete peak separation between DA and AA (for details, see the Supporting Information). This suggests that the ECNF sensor is selective for DA relative to AA and can distinguish between them.

dx.doi.org/10.1021/am405461j | ACS Appl. Mater. Interfaces 2014, 6, 3394−3405

CONCLUSIONS

We report the development of carbon-based electrochemical sensors with ultra-wide-range detection capabilities. The sensors consist of continuous defect-rich high-DOS ECNFs deposited on conductive substrates with good mesh integrity. The ESA of the ECNF sensor can be manipulated systematically by adjusting the electrospinning deposition time. This, in turn, allows us to adjust the LOD and dynamic range. The substrate-supported mesh architecture and ESA controllability of the ECNF sensor suggest its distinct advantage for wide-range electrochemical sensing over other carbon-based electrodes such as GC, CPE, carbon films, and CNT- and graphene-modified electrodes. The ECNF device exhibits a dynamic range $\sim 10^5$ greater than that of many existing biosensors for dopamine detection, indicating its excellent capability for ultra-wide-range sensing. The performance disparity between ECNFs and GFs highlights the pronounced advantage of using defect-rich high-DOS carbon materials with nanoscale crystallites for electrocatalysis applications. Because the electron-transfer efficiencies of many redox-active systems are governed by the DOS of the electrode materials, the ECNF sensing platform can be extended to a plethora of analytes in pharmaceutical, environmental, chemical, and biological industries, such as drugs, toxic metals, pesticides residuals, dye molecules, neurochemicals, proteins, and DNAs.[1,5,8−10]

EXPERIMENTAL SECTION

Materials. All chemicals were used as received. Polyacrylonitrile (PAN) (M_w = 150 000) was purchased from Polysciences. Potassium ferricyanide, dopamine hydrochloride, potassium chloride, sulfuric acid, and dimethylformamide (DMF) were purchased from Sigma-Aldrich. Ultrapure water (Milli-Q) was used in all of the experiments.

Fabrication of the ECNF Sensor. PAN was dissolved in DMF to form a 10 wt % solution in a 100 mL vial by vigorous stirring of the mixture for 2 h over a hot plate at 80 °C. Prior to electrospinning, the GF paper was coated with a thin PAN film by spin-coating the 10 wt % PAN/DMF solution onto the substrate at 1000 rpm for 2 min. Then, PAN fibers were electrospun directly onto the coated substrate using a parallel-plate apparatus. The applied potential, solution flow rate, and spin distance were 30 kV, 0.02 mL/min, and 30 cm, respectively. The as-spun polymer fibers attached to the substrate were stabilized in air at 270 °C for 1 h and then carbonized under nitrogen at an optimal temperature of 1200 °C[28] for 1 h (tube furnace, MTI, GSL-1800S60) to generate a high DOS. The heating rate was 5 °C/min from room temperature to 270 and 3 °C/min from 270 to 1200 °C. A load of 1.7 kPa was applied to the substrate/film/nanofiber construct using molybdenum plates during thermal treatment. In the absence of this applied pressure, the ECNF webs are somewhat fluffy and brittle.

Structural Characterization. Scanning electron microscopy (SEM) (JEOL-6060 SEM) was used for the morphological study of the carbon nanofibers. Samples for SEM were sputter-coated with a 10 nm layer of gold/palladium using a Desk II cold sputter/etch unit (Denton Vacuum LLC). X-ray diffraction (XRD) patterns were recorded using a PANalytical X'Pert Pro multipurpose diffractometer with Cu Kα radiation at a scanning speed of 3°/min between 5° and 50° (2θ). The XRD data analysis was performed using the HighScore Plus software package (PANalytical). X-ray photoelectron spectroscopy (XPS, Kratos Analytical) measurements were recorded with a Kratos Axis Ultra instrument equipped with a monochromatic Al Kα source operated at 150 W. The analyzer angle was set at 90° with respect to the specimen surface. The high-resolution spectra for C 1s core levels were recorded with steps of 0.1 eV and a pass energy of 20 eV. A Horiba Jobin Yvon Labram HR800 spectrometer (Horiba) was used for recording the Raman spectra using a 633 nm laser source at 3 mW of laser power. Transmission electron microscopy (TEM) (JEOL-2010 advanced high-performance TEM) was used to examine the surface nanostructures of the carbon nanofibers. The TEM samples were prepared by casting 2 μL of a suspension in water (1 mg/mL) of broken nanofibers generated by gentle sonication for 30 min onto a TEM grid. Ultraviolet photoemission spectra (UPS) were obtained using a He(I) emission lamp (21.2 eV photon energy) and collected at a 0.01 eV resolution with an electron takeoff angle of 90° and a pass energy of 0.585 eV. Gold was used as the internal reference sample.

Electrochemical Measurements. All of the electrochemical experiments were performed using an AutoLab PGSTAT 30 potentiostat with GPES software, version 4.9 (Eco Chemie). Voltammetric and impedance measurements were carried out with a standard three-electrode cell under argon protection and thermostatted at 25 ± 1 °C. A platinum wire and an Ag/AgCl (3 M NaCl) electrode (BASi) were used as auxiliary and reference electrodes, respectively. All potentials are referred to the Ag/AgCl electrode. The auxiliary and reference electrodes were rinsed with ethanol followed by ultrapure water before each experiment. For the impedance experiments, the frequency was varied from 0.1 to 10 000 Hz, and the potential was held at 0.3 V with a perturbation amplitude of 50 mV. For DA detection experiments, we employed the following procedure for adjusting the DA concentration stepwise from 0.2 to 100 000 μM in a single solution. Briefly, a three-necked flask was initially filled with 80 mL of blank electrolyte solution with zero DA concentration. First, four stock solutions with DA concentrations of 1, 0.1, 0.01, and 0.001 M were prepared. Next, an appropriate amount of the blank solution was replaced with the same volume of stock solutions to increase the DA concentration in the flask gradually while keeping constant the total volume of the solution in the flask. To measure the CVs at a DA concentration higher than 10^5 μM, it is more convenient to prepare separate solutions than to replace the working solution with the stock solution. This is because in the latter case a large volume of stock solution needs to be used and thus it is easier to use separate solutions. Cleaning of the GF electrode was performed using a previously reported procedure.[70] To prepare the activated carbon (AC)/solvent mixture, AC was mixed with water or acetonitrile in a 1:3 (v/v) AC/solvent ratio. The mixture was covered and allowed to stand for 30 min before use. Next, the electrode was immersed in the AC/solvent mixture for 10 min followed by an additional 10 min sonication in water. This treatment has been shown to be effective in removing adsorbed impurities from carbon surfaces because the large surface area of AC traps impurities.

ASSOCIATED CONTENT

Supporting Information

Calculation of the sp^3/sp^2 ratios from X-ray photoelectron spectroscopy, calculation of the R_I values from Raman spectroscopy, CV curves of $Fe(CN)_6^{3-/4-}$ at various scan rates, decay of the current response after multiple CV scans, selectivity of the ECNF sensor, discussion on the planar-diffusion behavior of $Fe(CN)_6^{3-/4-}$ of on the ECNF sensor during voltammetric measurements, dynamic range test for the GF electrode, and measurement of the capacitances of the GF electrode and the ECNF sensor. This material is available free of charge via the Internet at http://pubs.acs.org.

AUTHOR INFORMATION

Corresponding Authors

*E-mail: rutledge@mit.edu (G.C.R.).
*E-mail: tahatton@mit.edu (T.A.H.).

Present Address

†College of Electronics and Information Engineering, Sichuan University, Chengdu 610065, P. R. China.

Notes

The authors declare no competing financial interest.

■ ACKNOWLEDGMENTS

Xiaoqing Yang thanks the National Science Foundation of China (nos. 61001019 and 61372043) and the Major State Basic Research Development Program (nos. 2013CB328900 and 2013CB328905) for financial support.

■ REFERENCES

(1) Kimmel, D. W.; LeBlanc, G.; Meschievitz, M. E.; Cliffel, D. E. Electrochemical Sensors and Biosensors. *Anal. Chem.* **2012**, *84*, 685−707.
(2) McCreery, R. L. Advanced Carbon Electrode Materials for Molecular Electrochemistry. *Chem. Rev.* **2008**, *108*, 2646−2687.
(3) Qureshi, A.; Kang, W. P.; Davidson, J. L.; Gurbuz, Y. Review on Carbon-Derived, Solid-State, Micro and Nano Sensors for Electrochemical Sensing Applications. *Diamond Relat. Mater.* **2009**, *18*, 1401−1420.
(4) Ndamanisha, J. C.; Guo, L. P. Ordered Mesoporous Carbon for Electrochemical Sensing: A Review. *Anal. Chim. Acta* **2012**, *747*, 19−28.
(5) Vashist, S. K.; Zheng, D.; Al-Rubeaan, K.; Luong, J. H. T.; Sheu, F. S. Advances in Carbon Nanotube Based Electrochemical Sensors for Bioanalytical Applications. *Biotechnol. Adv.* **2011**, *29*, 169−188.
(6) Jacobs, C. B.; Peairs, M. J.; Venton, B. J. Review: Carbon Nanotube Based Electrochemical Sensors for Biomolecules. *Anal. Chim. Acta* **2010**, *662*, 105−127.
(7) Kuila, T.; Bose, S.; Khanra, P.; Mishra, A. K.; Kim, N. H.; Lee, J. H. Recent Advances in Graphene-Based Biosensors. *Biosens. Bioelectron.* **2011**, *26*, 4637−4648.
(8) Liu, Y. X.; Dong, X. C.; Chen, P. Biological and Chemical Sensors Based on Graphene Materials. *Chem. Soc. Rev.* **2012**, *41*, 2283−2307.
(9) Gupta, V. K.; Jain, R.; Radhapyari, K.; Jadon, N.; Agarwal, S. Voltammetric Techniques for the Assay of Pharmaceuticals − A Review. *Anal. Biochem.* **2011**, *408*, 179−196.
(10) Alghamdi, A. H. Applications of Stripping Voltammetric Techniques in Food Analysis. *Arabian J. Chem.* **2010**, *3*, 1−7.
(11) Zhang, M. N.; Yu, P.; Mao, L. Q. Rational Design of Surface/Interface Chemistry for Quantitative in Vivo Monitoring of Brain Chemistry. *Acc. Chem. Res.* **2012**, *45*, 533−543.
(12) Wilson, G. S.; Gifford, R. Biosensors for Real-Time in Vivo Measurements. *Biosens. Bioelectron.* **2005**, *20*, 2388−2403.
(13) Zhou, M.; Dong, S. J. Bioelectrochemical Interface Engineering: Toward the Fabrication of Electrochemical Biosensors, Biofuel Cells, and Self-Powered Logic Biosensors. *Acc. Chem. Res.* **2011**, *44*, 1232−1243.
(14) Wang, Y.; La, A.; Bruckner, C.; Lei, Y. Fret- and Pet-Based Sensing in a Single Material: Expanding the Dynamic Range of an Ultra-Sensitive Nitroaromatic Explosives Assay. *Chem. Commun.* **2012**, *48*, 9903−9905.
(15) Kim, Y. R.; Bong, S.; Kang, Y. J.; Yang, Y.; Mahajan, R. K.; Kim, J. S.; Kim, H. Electrochemical Detection of Dopamine in the Presence of Ascorbic Acid Using Graphene Modified Electrodes. *Biosens. Bioelectron.* **2010**, *25*, 2366−2369.
(16) Sun, C. L.; Chang, C. T.; Lee, H. H.; Zhou, J. G.; Wang, J.; Sham, T. K.; Pong, W. F. Microwave-Assisted Synthesis of a Core-Shell MWCNT/GONR Heterostructure for the Electrochemical Detection of Ascorbic Acid, Dopamine, and Uric Acid. *ACS Nano* **2011**, *5*, 7788−7795.
(17) Qin, S. H.; Qin, D. Q.; Ford, W. T.; Zhang, Y. J.; Kotov, N. A. Covalent Cross-Linked Polymer/Single-Wall Carbon Nanotube Multilayer Films. *Chem. Mater.* **2005**, *17*, 2131−2135.
(18) Gong, K. P.; Zhang, M. N.; Yan, Y. M.; Su, L.; Mao, L. Q.; Xiong, Z. X.; Chen, Y. Sol-Gel-Derived Ceramic-Carbon Nanotube Nanocomposite Electrodes: Tunable Electrode Dimension and Potential Electrochemical Applications. *Anal. Chem.* **2004**, *76*, 6500−6505.
(19) Profumo, A.; Fagnoni, M.; Merli, D.; Quartarone, E.; Protti, S.; Dondi, D.; Albini, A. Multiwalled Carbon Nanotube Chemically Modified Gold Electrode for Inorganic as Speciation and Bi(III) Determination. *Anal. Chem.* **2006**, *78*, 4194−4199.
(20) Li, Y. X.; Wang, P.; Wang, L.; Lin, X. Q. Overoxidized Polypyrrole Film Directed Single-Walled Carbon Nanotubes Immobilization on Glassy Carbon Electrode and Its Sensing Applications. *Biosens. Bioelectron.* **2007**, *22*, 3120−3125.
(21) Kelly, R. S.; Weiss, D. J.; Chong, S. H.; Kuwana, T. Charge Selective Electrochemistry at High-Surface Area Carbon Fibers. *Anal. Chem.* **1999**, *71*, 413−418.
(22) Kelly, R. S.; Coleman, B. D.; Huang, T.; Inkaew, P.; Kuwana, T. Electrochemical Flow Injection Analysis Study of Ion Partitioning at High Surface Area Carbon Fiber Electrodes. *Anal. Chem.* **2002**, *74*, 6364−6369.
(23) Dzenis, Y. Spinning Continuous Fibers for Nanotechnology. *Science* **2004**, *304*, 1917−1919.
(24) Inagaki, M.; Yang, Y.; Kang, F. Y. Carbon Nanofibers Prepared via Electrospinning. *Adv. Mater.* **2012**, *24*, 2547−2566.
(25) Mao, X.; Hatton, T. A.; Rutledge, G. C. A Review of Electrospun Carbon Fibers as Electrode Materials for Energy Storage. *Curr. Org. Chem.* **2013**, *17*, 1390−1401.
(26) Huang, J. S.; Wang, D. W.; Hou, H. Q.; You, T. Y. Electrospun Palladium Nanoparticle-Loaded Carbon Nanofibers and Their Electrocatalytic Activities towards Hydrogen Peroxide and NADH. *Adv. Funct. Mater.* **2008**, *18*, 441−448.
(27) Hu, G. Z.; Zhou, Z. P.; Guo, Y.; Hou, H. Q.; Shao, S. J. Electrospun Rhodium Nanoparticle-Loaded Carbon Nanofibers for Highly Selective Amperometric Sensing of Hydrazine. *Electrochem. Commun.* **2010**, *12*, 422−426.
(28) Mao, X.; Simeon, F.; Rutledge, G. C.; Hatton, T. A. Electrospun Carbon Nanofiber Webs with Controlled Density of States for Sensor Applications. *Adv. Mater.* **2013**, *25*, 1309−1314.
(29) Wang, Y. L.; Zhu, Y. C.; Chen, J. J.; Zeng, Y. Amperometric Biosensor Based on 3D Ordered Freestanding Porous Pt Nanowire Array Electrode. *Nanoscale* **2012**, *4*, 6025−6031.
(30) Lu, W. B.; Qin, X. Y.; Asiri, A. M.; Al-Youbi, A. O.; Sun, X. P. Ni Foam: A Novel Three-Dimensional Porous Sensing Platform for Sensitive and Selective Nonenzymatic Glucose Detection. *Analyst* **2013**, *138*, 417−420.
(31) Pan, L. J.; Yu, G. H.; Zhai, D. Y.; Lee, H. R.; Zhao, W. T.; Liu, N.; Wang, H. L.; Tee, B. C. K.; Shi, Y.; Cui, Y.; Bao, Z. N. Hierarchical Nanostructured Conducting Polymer Hydrogel with High Electrochemical Activity. *Proc. Natl. Acad. Sci. U.S.A.* **2012**, *109*, 9287−9292.
(32) Leger, C.; Bertrand, P. Direct Electrochemistry of Redox Enzymes as a Tool for Mechanistic Studies. *Chem. Rev.* **2008**, *108*, 2379−2438.
(33) Heien, M. L. A. V.; Khan, A. S.; Ariansen, J. L.; Cheer, J. F.; Phillips, P. E. M.; Wassum, K. M.; Wightman, R. M. Real-Time Measurement of Dopamine Fluctuations after Cocaine in the Brain of Behaving Rats. *Proc. Natl. Acad. Sci. U.S.A.* **2005**, *102*, 10023−10028.
(34) Tye, K. M.; Mirzabekov, J. J.; Warden, M. R.; Ferenczi, E. A.; Tsai, H. C.; Finkelstein, J.; Kim, S. Y.; Adhikari, A.; Thompson, K. R.; Andalman, A. S.; Gunaydin, L. A.; Witten, I. B.; Deisseroth, K. Dopamine Neurons Modulate Neural Encoding and Expression of Depression-Related Behaviour. *Nature* **2013**, *493*, 537−541.
(35) Wightman, R. M.; May, L. J.; Michael, A. C. Detection of Dopamine Dynamics in the Brain. *Anal. Chem.* **1988**, *60*, A769−A779.
(36) Carlsson, A.; Lindqvist, M.; Magnusson, T. 3,4-Dihydroxyphenylalanine and 5-Hydroxytryptophan as Reserpine Antagonists. *Nature* **1957**, *180*, 1200−1200.
(37) Savitt, J. M.; Dawson, V. L.; Dawson, T. M. Diagnosis and Treatment of Parkinson Disease: Molecules to Medicine. *J. Clin. Invest.* **2006**, *116*, 1744−1754.
(38) Cao, X. H.; Zhang, L. X.; Cai, W. P.; Li, Y. Q. Amperometric Sensing of Dopamine Using a Single-Walled Carbon Nanotube Covalently Attached to a Conical Glass Micropore Electrode. *Electrochem. Commun.* **2010**, *12*, 540−543.
(39) Min, K.; Yoo, Y. J. Amperometric Detection of Dopamine Based on Tyrosinase-SWNTs-Ppy Composite Electrode. *Talanta* **2009**, *80*, 1007−1011.

(40) Zheng, D.; Ye, J. S.; Zhang, W. D. Some Properties of Sodium Dodecyl Sulfate Functionalized Multiwalled Carbon Nanotubes Electrode and Its Application on Detection of Dopamine in the Presence of Ascorbic Acid. *Electroanalysis* **2008**, *20*, 1811−1818.
(41) Shahrokhian, S.; Zare-Mehrjardi, H. R. Application of Thionine-Nation Supported on Multi-Walled Carbon Nanotube for Preparation of a Modified Electrode in Simultaneous Voltammetric Detection of Dopamine and Ascorbic Acid. *Electrochim. Acta* **2007**, *52*, 6310−6317.
(42) Yogeswaran, U.; Chen, S. M. Multi-Walled Carbon Nanotubes with Poly(Methylene Blue) Composite Film for the Enhancement and Separation of Electroanalytical Responses of Catecholamine and Ascorbic Acid. *Sens. Actuators, B* **2008**, *130*, 739−749.
(43) Zhang, Y. Z.; Pan, Y.; Sit, S.; Zhang, L. P.; Li, S. P.; Shao, M. W. A Novel Functionalized Single-Wall Carbon Nanotube Modified Electrode and Its Application in Determination of Dopamine and Uric Acid in the Presence of High Concentrations of Ascorbic Acid. *Electroanalysis* **2007**, *19*, 1695−1701.
(44) Kan, X. W.; Zhao, Y.; Geng, Z. R.; Wang, Z. L.; Zhu, J. J. Composites of Multiwalled Carbon Nanotubes and Molecularly Imprinted Polymers for Dopamine Recognition. *J. Phys. Chem. C* **2008**, *112*, 4849−4854.
(45) Xiang, L.; Lin, Y. Q.; Yu, P.; Su, L.; Mao, L. Q. Laccase-Catalyzed Oxidation and Intramolecular Cyclization of Dopamine: A New Method for Selective Determination of Dopamine with Laccase/Carbon Nanotube-Based Electrochemical Biosensors. *Electrochim. Acta* **2007**, *52*, 4144−4152.
(46) Tsai, Y. C.; Chiu, C. C. Amperometric Biosensors Based on Multiwalled Carbon Nanotube-Nafion-Tyrosinase Nanobiocomposites for the Determination of Phenolic Compounds. *Sens. Actuators, B* **2007**, *125*, 10−16.
(47) Manjunatha, R.; Suresh, G. S.; Melo, J. S.; D'Souza, S. F.; Venkatesha, T. V. Simultaneous Determination of Ascorbic Acid, Dopamine and Uric Acid Using Polystyrene Sulfonate Wrapped Multiwalled Carbon Nanotubes Bound to Graphite Electrode through Layer-by-Layer Technique. *Sens. Actuators, B* **2010**, *145*, 643−650.
(48) Alothman, Z. A.; Bukhari, N.; Wabaidur, S. M.; Haider, S. Simultaneous Electrochemical Determination of Dopamine and Acetaminophen Using Multiwall Carbon Nanotubes Modified Glassy Carbon Electrode. *Sens. Actuators, B* **2010**, *146*, 314−320.
(49) Liu, S. Q.; Sun, W. H.; Hu, F. T. Graphene Nano Sheet-Fabricated Electrochemical Sensor for the Determination of Dopamine in the Presence of Ascorbic Acid Using Cetyltrimethylammonium Bromide as the Discriminating Agent. *Sens. Actuators, B* **2012**, *173*, 497−504.
(50) Liu, X.; Xie, L. L.; Li, H. L. Electrochemical Biosensor Based on Reduced Graphene Oxide and Au Nanoparticles Entrapped in Chitosan/Silica Sol-Gel Hybrid Membranes for Determination of Dopamine and Uric Acid. *J. Electroanal. Chem.* **2012**, *682*, 158−163.
(51) Liu, Q.; Zhu, X.; Huo, Z. H.; He, X. L.; Liang, Y.; Xu, M. T. Electrochemical Detection of Dopamine in the Presence of Ascorbic Acid Using PVP/Graphene Modified Electrodes. *Talanta* **2012**, *97*, 557−562.
(52) Han, D. X.; Han, T. T.; Shan, C. S.; Ivaska, A.; Niu, L. Simultaneous Determination of Ascorbic Acid, Dopamine and Uric Acid with Chitosan-Graphene Modified Electrode. *Electroanalysis* **2010**, *22*, 2001−2008.
(53) Zhang, Y.; Yuan, R.; Chai, Y. Q.; Li, W. J.; Zhong, X.; Zhong, H. A. Simultaneous Voltammetric Determination for Da, Aa and No2-Based on Graphene/Poly-Cyclodextrin/MWCNTs Nanocomposite Platform. *Biosens. Bioelectron.* **2011**, *26*, 3977−3980.
(54) Kim, C.; Yang, K. S.; Kojima, M.; Yoshida, K.; Kim, Y. J.; Kim, Y. A.; Endo, M. Fabrication of Electrospinning-Derived Carbon Nanofiber Webs for the Anode Material of Lithium-Ion Secondary Batteries. *Adv. Funct. Mater.* **2006**, *16*, 2393−2397.
(55) Iwashita, N.; Park, C. R.; Fujimoto, H.; Shiraishi, M.; Inagaki, M. Specification for a Standard Procedure of X-ray Diffraction Measurements on Carbon Materials. *Carbon* **2004**, *42*, 701−714.
(56) Estrade-Szwarckopf, H. XPS Photoemission in Carbonaceous Materials: A "Defect" Peak Beside the Graphitic Asymmetric Peak. *Carbon* **2004**, *42*, 1713−1721.
(57) Pimenta, M. A.; Dresselhaus, G.; Dresselhaus, M. S.; Cancado, L. G.; Jorio, A.; Saito, R. Studying Disorder in Graphite-Based Systems by Raman Spectroscopy. *Phys. Chem. Chem. Phys.* **2007**, *9*, 1276−1291.
(58) Koivusaari, K. J.; Rantala, T. T.; Leppavuori, S. Calculated Electronic Density of States and Structural Properties of Tetrahedral Amorphous Carbon. *Diamond Relat. Mater.* **2000**, *9*, 736−740.
(59) Wiggins-Camacho, J. D.; Stevenson, K. J. Effect of Nitrogen Concentration on Capacitance, Density of States, Electronic Conductivity, and Morphology of N-Doped Carbon Nanotube Electrodes. *J. Phys. Chem. C* **2009**, *113*, 19082−19090.
(60) McFeely, F. R.; Kowalczy, Sp; Ley, L.; Cavell, R. G.; Pollak, R. A.; Shirley, D. A. X-ray Photoemission Studies of Diamond, Graphite, and Glassy Carbon Valence Bands. *Phys. Rev. B* **1974**, *9*, 5268−5278.
(61) Royea, W. J.; Hamann, T. W.; Brunschwig, B. S.; Lewis, N. S. A Comparison between Interfacial Electron-Transfer Rate Constants at Metallic and Graphite Electrodes. *J. Phys. Chem. B* **2006**, *110*, 19433−19442.
(62) Banks, C. E.; Compton, R. G. New Electrodes for Old: From Carbon Nanotubes to Edge Plane Pyrolytic Graphite. *Analyst* **2006**, *131*, 15−21.
(63) McDermott, M. T.; Kneten, K.; McCreery, R. L. Anthraquinonedisulfonate Adsorption, Electron-Transfer Kinetics, and Capacitance on Ordered Graphite-Electrodes: The Important Role of Surface-Defects. *J. Phys. Chem.* **1992**, *96*, 3124−3130.
(64) Yuan, W. J.; Zhou, Y.; Li, Y. R.; Li, C.; Peng, H. L.; Zhang, J.; Liu, Z. F.; Dai, L. M.; Shi, G. Q. The Edge- and Basal-Plane-Specific Electrochemistry of a Single-Layer Graphene Sheet. *Sci. Rep.* **2013**, *3*, 2248.
(65) Davies, T. J.; Hyde, M. E.; Compton, R. G. Nanotrench Arrays Reveal Insight into Graphite Electrochemistry. *Angew. Chem., Int. Ed.* **2005**, *44*, 5121−5126.
(66) Bowling, R. J.; Packard, R. T.; Mccreery, R. L. Activation of Highly Ordered Pyrolytic-Graphite for Heterogeneous Electron Transfer: Relationship between Electrochemical Performance and Carbon Microstructure. *J. Am. Chem. Soc.* **1989**, *111*, 1217−1223.
(67) Ji, X. B.; Banks, C. E.; Crossley, A.; Compton, R. G. Oxygenated Edge Plane Sites Slow the Electron Transfer of the Ferro-/Ferricyanide Redox Couple at Graphite Electrodes. *ChemPhysChem* **2006**, *7*, 1337−1344.
(68) Banks, C. E.; Moore, R. R.; Davies, T. J.; Compton, R. G. Investigation of Modified Basal Plane Pyrolytic Graphite Electrodes: Definitive Evidence for the Electrocatalytic Properties of the Ends of Carbon Nanotubes. *Chem. Commun.* **2004**, 1804−1805.
(69) Chen, P. H.; McCreery, R. L. Control of Electron Transfer Kinetics at Glassy Carbon Electrodes by Specific Surface Modification. *Anal. Chem.* **1996**, *68*, 3958−3965.
(70) Ranganathan, S.; Kuo, T. C.; McCreery, R. L. Facile Preparation of Active Glassy Carbon Electrodes with Activated Carbon and Organic Solvents. *Anal. Chem.* **1999**, *71*, 3574−3580.
(71) Shalini, J.; Sankaran, K. J.; Dong, C. L.; Lee, C. Y.; Tai, N. H.; Lin, I. N. In Situ Detection of Dopamine Using Nitrogen Incorporated Diamond Nanowire Electrode. *Nanoscale* **2013**, *5*, 1159−1167.
(72) Hrapovic, S.; Liu, Y. L.; Male, K. B.; Luong, J. H. T. Electrochemical Biosensing Platforms Using Platinum Nanoparticles and Carbon Nanotubes. *Anal. Chem.* **2004**, *76*, 1083−1088.
(73) DuVall, S. H.; McCreery, R. L. Self-Catalysis by Catechols and Quinones During Heterogeneous Electron Transfer at Carbon Electrodes. *J. Am. Chem. Soc.* **2000**, *122*, 6759−6764.
(74) Takmakov, P.; Zachek, M. K.; Keithley, R. B.; Walsh, P. L.; Donley, C.; McCarty, G. S.; Wightman, R. M. Carbon Microelectrodes with a Renewable Surface. *Anal. Chem.* **2010**, *82*, 2020−2028.
(75) Laviron, E. General Expression of the Linear Potential Sweep Voltammogram in the Case of Diffusionless Electrochemical Systems. *J. Electroanal. Chem.* **1979**, *101*, 19−28.
(76) Yang, J.; Strickler, J. R.; Gunasekaran, S. Indium Tin Oxide-Coated Glass Modified with Reduced Graphene Oxide Sheets and

Gold Nanoparticles as Disposable Working Electrodes for Dopamine Sensing in Meat Samples. *Nanoscale* **2012**, *4*, 4594−4602.
(77) Wang, Y.; Li, Y. M.; Tang, L. H.; Lu, J.; Li, J. H. Application of Graphene-Modified Electrode for Selective Detection of Dopamine. *Electrochem. Commun.* **2009**, *11*, 889−892.
(78) Hou, S. F.; Kasner, M. L.; Su, S. J.; Patel, K.; Cuellari, R. Highly Sensitive and Selective Dopamine Biosensor Fabricated with Silanized Graphene. *J. Phys. Chem. C* **2010**, *114*, 14915−14921.
(79) Deng, C. Y.; Chen, J. H.; Wang, M. D.; Xiao, C. H.; Nie, Z.; Yao, S. Z. A Novel and Simple Strategy for Selective and Sensitive Determination of Dopamine Based on the Boron-Doped Carbon Nanotubes Modified Electrode. *Biosens. Bioelectron.* **2009**, *24*, 2091−2094.